

# Comparing effective temperatures in standard, Tsallis, and q-dual statistics from transverse momentum spectra of identified light charged hadrons produced in gold–gold collisions at RHIC energies

Ting-Ting Duan<sup>1,\*</sup>, Pei-Pin Yang<sup>2,†</sup>, Peng-Cheng Zhang<sup>1,‡</sup>,  
 Hai-Ling Lao<sup>3,§</sup>, Fu-Hu Liu<sup>1,¶</sup>, Khusniddin K. Olimov<sup>4,5,\*\*</sup>

<sup>1</sup>*Institute of Theoretical Physics, State Key Laboratory of Quantum Optics and Quantum Optics Devices & Collaborative Innovation Center of Extreme Optics, Shanxi University, Taiyuan 030006, China*

<sup>2</sup>*Department of Physics, Xinzhou Normal University, Xinzhou 034000, China*

<sup>3</sup>*Department of Science Teaching, Beijing Vocational College of Agriculture, Beijing 102442, China*

<sup>4</sup>*Laboratory of High Energy Physics, Physical-Technical Institute of Uzbekistan Academy of Sciences, Chingiz Aytmatov Str. 2b, Tashkent 100084, Uzbekistan*

<sup>5</sup>*Department of Natural Sciences, National University of Science and Technology MISIS (NUST MISIS), Almalyk Branch, Almalyk 110105, Uzbekistan*

**Abstract:** This study investigates the transverse momentum ( $p_T$ ) spectra of identified light charged hadrons produced in gold–gold (Au+Au) collisions across various centrality classes at center-of-mass energies per nucleon pair,  $\sqrt{s_{NN}}$ , ranging from 7.7 to 200 GeV, as measured by the STAR Collaboration at the Relativistic Heavy Ion Collider (RHIC). The analysis employs standard (Bose-Einstein/Fermi-Dirac), Tsallis, and q-dual statistics to fit the same  $p_T$  spectra and derive distinct effective temperatures:  $T_{\text{Standard}}$ ,  $T_{\text{Tsallis}}$ , and  $T_{\text{q-dual}}$ . In most instances, there exists an approximately linear relationship or positive correlation between  $T_{\text{Tsallis}}$  and  $T_{\text{Standard}}$ , as well as between  $T_{\text{q-dual}}$  and  $T_{\text{Standard}}$ , when considering  $T_{\text{Standard}}$  as a baseline. However, while both  $T_{\text{Tsallis}}$  and  $T_{\text{q-dual}}$  increase from semi-central to central Au+Au collisions at 62.4 GeV and 200 GeV, where QGP is expected, changes in  $T_{\text{Standard}}$  occur more gradually. This work suggests that  $T_{\text{Standard}}$  is better suited for characterizing phase transitions between hadronic matter and QGP compared to  $T_{\text{Tsallis}}$  or  $T_{\text{q-dual}}$ , primarily due to the considerations related to entropy index in the Tsallis and q-dual statistics.

**Keywords:** Standard (Bose-Einstein/Fermi-Dirac) distribution, Tsallis distribution, q-dual distribution, effective temperatures

**PACS Nos:** 12.40.Ee, 13.85.Hd, 24.10.Pa

## I. INTRODUCTION

As one of the most fundamental concepts, temperature is extensively utilized in both scientific research and everyday life [1]. To obtain temperature values, a thermometer is essential. Different types of thermometers exist based on various temperature scales, allowing for conversion between the measurements obtained from different devices. However, not all thermometers are capable of measuring temperatures across a broad range; indeed, some

---

\* 202312602001@email.sxu.edu.cn

† peipinyangshanxi@163.com; peipinyang@xztu.edu.cn

‡ 202312602003@email.sxu.edu.cn

§ hailinglao@163.com; hailinglao@pku.edu.cn

¶ Correspondence: fuhuliu@163.com; fuhuliu@sxu.edu.cn

\*\* Correspondence: khkolimov@gmail.com; kh.olimov@uzsci.net

have very limited measurement capabilities. To address this limitation and measure temperatures over an extensive range, multiple thermometers can be employed concurrently. This necessitates coordination and conversion among the readings from different thermometers to facilitate meaningful comparisons.

In particular, applying the concept of temperature in high-energy collisions presents challenges for researchers due to inconsistent definitions and methodologies. Various types of temperatures exist within this context, including but not limited to initial state temperature, chemical freeze-out temperature, kinetic freeze-out temperature, and effective temperature in high-energy collisions [2–7]. As their names suggest: initial state temperature describes the excitation degrees at the onset of collisions; chemical freeze-out temperature pertains to conditions when particle interactions cease; while kinetic freeze-out temperature reflects states where particles no longer interact significantly during their motion. The effective temperature indicates the average kinetic energy or transverse momentum of multiple particles at the stage of kinetic freeze-out while accounting for flow effects.

Indeed, average kinetic energy arises from both thermal motion among numerous particles and collective motion originating from emission sources or groups of particles. The former is characterized by kinetic freeze-out temperatures whereas the latter is represented through transverse flow velocity. Here, the longitudinal motion of the emission source is not considered; rather, it is assumed that the emission source remains in its rest frame. Due to limitations in time and space scales, direct measurements of temperatures in high-energy collisions using conventional thermometers are not feasible. Instead, the community employs indirect methods based on yield ratios and transverse momentum ( $p_T$ ) spectra of multiple particles.

The chemical freeze-out temperature can be “measured” through yield ratios. The “measurements” pertaining to initial state, kinetic freeze-out, and effective temperatures rely on  $p_T$  spectra. Various functions incorporating temperature parameters can be utilized to fit these  $p_T$  spectra; here, the temperature parameters represent effective temperatures. By introducing transverse flow velocity into these functions, one can derive the kinetic freeze-out temperature from the  $p_T$  spectra. Utilizing average  $p_T$  ( $\langle p_T \rangle$ ) and root-mean-square  $p_T$  ( $\sqrt{\langle p_T^2 \rangle}$ ), both kinetic freeze-out and initial state temperatures can be extracted according to thermal-related methodologies [8] as well as string percolation models [9–11], respectively.

It is important to note that the type of temperature discussed in high-energy collisions may exhibit model dependence [12–15]. For instance, effective temperatures derived from standard (Bose-Einstein/Fermi-Dirac), Tsallis statistics, and q-dual statistics differ significantly [16–19]. While it is acknowledged that certain thermal or Tsallis distributions can effectively fit experimental data, exploring the relationships between different effective temperatures warrants further investigation. Establishing such relationships will facilitate baseline comparisons across various models. The primary focus of this work lies in comparing different effective temperatures.

One can reasonably assume that there exist linear relationships between  $T_{\text{Tsallis}}$  and  $T_{\text{Standard}}$ , as well as between  $T_{\text{q-dual}}$  and  $T_{\text{Standard}}$ , when considering  $T_{\text{Standard}}$  as a baseline. To investigate the relationships among different effective temperatures, we will analyze the production of identified light charged hadrons ( $\pi^+$ ,  $\pi^-$ ,  $K^+$ ,  $K^-$ ,  $p$ , and  $\bar{p}$ ) produced in gold–gold (Au+Au) collisions at center-of-mass energies per nucleon pair of  $\sqrt{s_{NN}} = 7.7, 11.5, 19.6, 27, 39, 62.4,$  and  $200$  GeV. These measurements were conducted by the STAR Collaboration [20–22] at the Relativistic Heavy Ion Collider (RHIC). The functions related to  $p_T$  derived from standard statistics, Tsallis statistics, and q-dual statistics are employed to extract various effective temperatures.

The remainder of this paper is organized as follows: Section 2 describes the multi-source picture and formalism associated with different functions; Section 3 presents our results and discussion; finally, Section 4 provides a summary and conclusions.

## II. MULTI-SOURCE PICTURE AND FORMULISM

Within the framework of a multi-source thermal model [23–25], it can be posited that multiple emission sources arise in high-energy collisions due to varying excitation degrees or interaction mechanisms. This multi-source nature allows for representation in terms of a multi-component form. For each individual emission source, distinct models

or functions may be utilized to describe particle production effectively. Naturally and conveniently chosen for this purpose is the relativistic ideal gas model within standard statistics for characterizing multiple particles produced from each source.

The application of the relativistic ideal gas model with temperature  $T$  yields an expression for the total number of particles given by [19].

$$N = gV \int \frac{d^3p}{(2\pi)^3} \left[ \exp\left(\frac{E - \mu}{T}\right) + S \right]^{-1}, \quad (1)$$

where  $g$  is the degeneracy factor, which equals 1 for bosons such as  $\pi^\pm$  and  $K^\pm$ , and 2 for fermions such as  $p(\bar{p})$ .  $V$  represents the volume of the collision system,  $p$  denotes momentum,

$$E = \sqrt{p^2 + m_0^2} = m_T \cosh y \quad (2)$$

signifies energy,  $m_0$  indicates rest mass,

$$m_T = \sqrt{p_T^2 + m_0^2} \quad (3)$$

refers to transverse mass,

$$y = \frac{1}{2} \ln \left( \frac{E + p_z}{E - p_z} \right) \quad (4)$$

stands for rapidity, while  $p_z$  corresponds to longitudinal momentum. The chemical potential of the considered particles is denoted by  $\mu$ . In the latter part of this equation, we have that  $S = -1$ , which corresponds to Bose-Einstein statistics applicable to bosons; conversely, when  $S = 1$ , it pertains to Fermi-Dirac statistics relevant for fermions. As an approximation, setting  $S = 0$  aligns with Maxwell-Boltzmann statistics.

The invariant yield or momentum spectrum of the considered particles is written as [19]

$$E \frac{d^3N}{d^3p} = \frac{1}{2\pi p_T} \frac{d^2N}{dy dp_T} = \frac{1}{2\pi m_T} \frac{d^2N}{dy dm_T} = \frac{gV}{(2\pi)^3} E \left[ \exp\left(\frac{E - \mu}{T}\right) + S \right]^{-1}. \quad (5)$$

The density function of momenta can be given by

$$\frac{dN}{dp} = \frac{2gV}{(2\pi)^2} p^2 \left[ \exp\left(\frac{\sqrt{p^2 + m_0^2} - \mu}{T}\right) + S \right]^{-1}. \quad (6)$$

The unit-density function of  $y$  and  $p_T$  is written as [19]

$$\frac{d^2N}{dy dp_T} = \frac{gV}{(2\pi)^2} p_T \sqrt{p_T^2 + m_0^2} \cosh y \left[ \exp\left(\frac{\sqrt{p_T^2 + m_0^2} \cosh y - \mu}{T}\right) + S \right]^{-1}. \quad (7)$$

From the unit-density function Eq. (7), the density function of  $p_T$  is given by

$$\frac{dN}{dp_T} = \frac{gV}{(2\pi)^2} p_T \sqrt{p_T^2 + m_0^2} \int_{y_{\min}}^{y_{\max}} \cosh y \left[ \exp\left(\frac{\sqrt{p_T^2 + m_0^2} \cosh y - \mu}{T}\right) + S \right]^{-1} dy. \quad (8)$$

Here,  $E$  appears in terms of  $y$  and  $p_T$  due to the integration for  $y$ . The experimental rapidity bin  $[y_{\min}, y_{\max}]$  is considered as the lower and upper limits of the integration. The density function of  $y$  is

$$\frac{dN}{dy} = \frac{gV}{(2\pi)^2} \int_0^{p_{T \max}} p_T \sqrt{p_T^2 + m_0^2} \cosh y \left[ \exp\left(\frac{\sqrt{p_T^2 + m_0^2} \cosh y - \mu}{T}\right) + S \right]^{-1} dp_T, \quad (9)$$

where  $p_{T \max}$  denotes the maximum  $p_T$  in experiments, though it is infinity in mathematics.

Considering the multi-source thermal model [23–25] which results in a multi-component form which reflects a multi-region structure of  $p_T$  spectra [26–28], one has some distributions in the multi-component form as followings

$$N = \sum_{i=1}^{n_0} N_i, \quad (10)$$

$$E \frac{d^3 N}{d^3 p} = \sum_{i=1}^{n_0} E \frac{d^3 N_i}{d^3 p}, \quad (11)$$

$$\frac{dN}{dp} = \sum_{i=1}^{n_0} \frac{dN_i}{dp}, \quad (12)$$

$$\frac{d^2 N}{dy dp_T} = \sum_{i=1}^{n_0} \frac{d^2 N_i}{dy dp_T}, \quad (13)$$

$$\frac{dN}{dp_T} = \sum_{i=1}^{n_0} \frac{dN_i}{dp_T}, \quad (14)$$

$$\frac{dN}{dy} = \sum_{i=1}^{n_0} \frac{dN_i}{dy}, \quad (15)$$

where  $i$  denotes the  $i$ -th component in  $n_0$  components and  $N_i$  is the number of particles in the  $i$ -th component.

In a multi-component framework, various components can be expressed in a similar form due to their commonality [29–32] and universality [33–36] observed in high-energy collisions. From the first component through to the last one within this multi-component structure reveals a decrease in fraction alongside an increase in temperature. The average temperature is represented by

$$T = \sum_{i=1}^{n_0} k_i T_i, \quad (16)$$

where  $k_i = N_i/N$  is defined as the contribution ratio or fraction of the  $i$ -th component among a total of  $n_0$  components with corresponding temperature denoted by  $T_i$ . Naturally,  $\sum_{i=1}^{n_0} k_i = 1$  must hold true.

The multi-component distributions in the standard statistics can be empirically covered by the distributions in the Tsallis statistics which has the following related equations [14–18]

$$N = gV \int \frac{d^3 p}{(2\pi)^3} \left\{ \left[ 1 + (q-1) \frac{E - \mu}{T} \right]^{\frac{1}{q-1}} + S \right\}^{-q}, \quad (17)$$

$$E \frac{d^3 N}{d^3 p} = \frac{gV}{(2\pi)^3} E \left\{ \left[ 1 + (q-1) \frac{E - \mu}{T} \right]^{\frac{1}{q-1}} + S \right\}^{-q}, \quad (18)$$

$$\frac{dN}{dp} = \frac{2gV}{(2\pi)^2} p^2 \left\{ \left[ 1 + (q-1) \frac{\sqrt{p^2 + m_0^2} - \mu}{T} \right]^{\frac{1}{q-1}} + S \right\}^{-q}, \quad (19)$$

$$\frac{d^2 N}{dy dp_T} = \frac{gV}{(2\pi)^2} p_T \sqrt{p_T^2 + m_0^2} \cosh y \left\{ \left[ 1 + (q-1) \frac{\sqrt{p_T^2 + m_0^2} \cosh y - \mu}{T} \right]^{\frac{1}{q-1}} + S \right\}^{-q}, \quad (20)$$

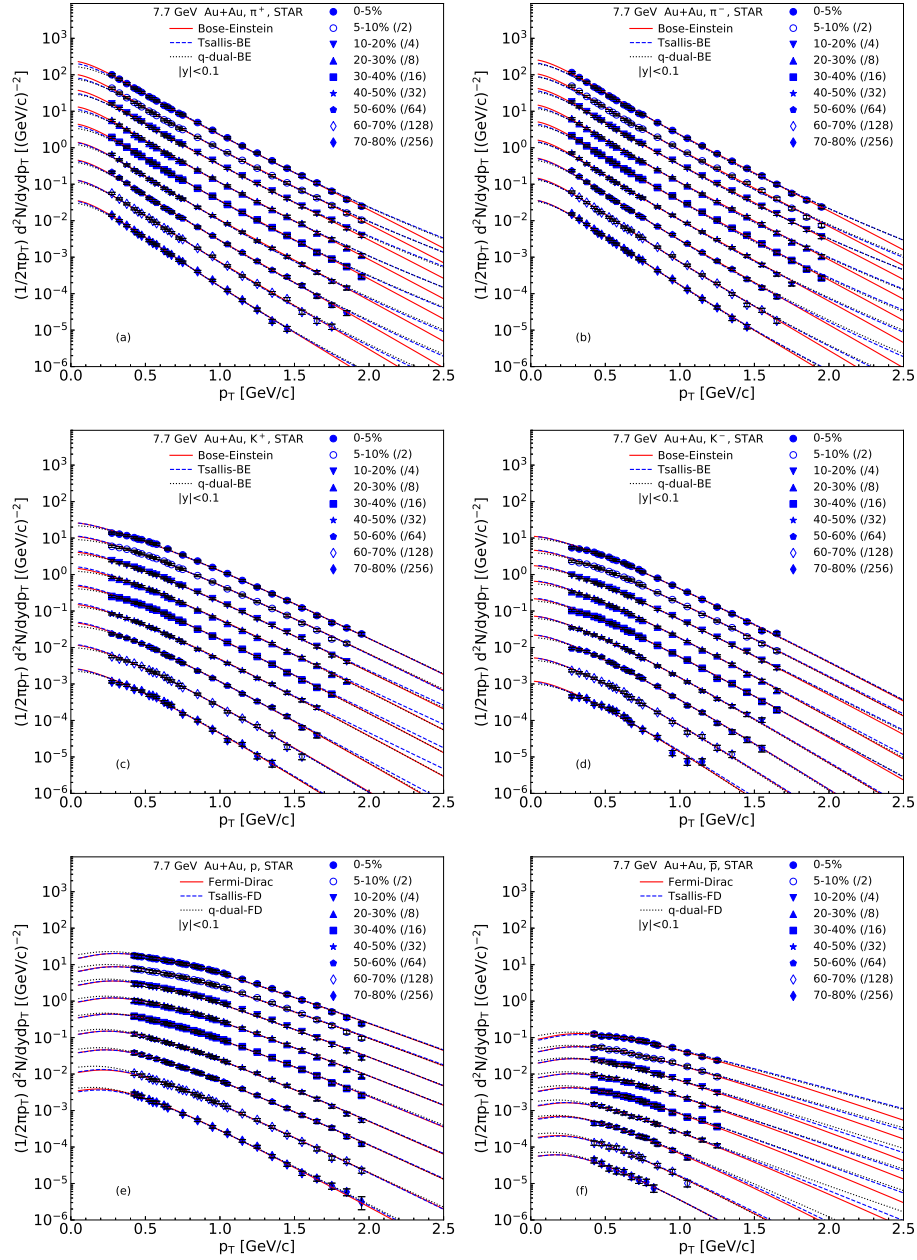


Figure 1. The invariant yields,  $(1/2\pi p_T)d^2N/dydp_T$ , of (a)  $\pi^+$ , (b)  $\pi^-$ , (c)  $K^+$ , (d)  $K^-$ , (e)  $p$ , and (f)  $\bar{p}$  produced in  $|y| < 0.1$  in Au+Au collisions at  $\sqrt{s_{NN}} = 7.7$  GeV. Different symbols represent the experimental data measured by the STAR Collaboration [20] at RHIC. There are nine centrality percentage classes (0–5%, 5–10%, 10–20%, 20–30%, 30–40%, 40–50%, 50–60%, 60–70%, and 70–80%) being used. For each centrality percentage class, the data are scaled by a given quantity shown in the panel for clear display. The solid, dashed, and dotted curves are our results fitted by the distributions from the standard, Tsallis, and q-dual statistics, respectively.

$$\frac{dN}{dp_T} = \frac{gV}{(2\pi)^2} p_T \sqrt{p_T^2 + m_0^2} \int_{y_{\min}}^{y_{\max}} \cosh y \left\{ \left[ 1 + (q-1) \frac{\sqrt{p_T^2 + m_0^2} \cosh y - \mu}{T} \right]^{\frac{1}{q-1}} + S \right\}^{-q} dy, \quad (21)$$

$$\frac{dN}{dy} = \frac{gV}{(2\pi)^2} \int_0^{p_T^{\max}} p_T \sqrt{p_T^2 + m_0^2} \cosh y \left\{ \left[ 1 + (q-1) \frac{\sqrt{p_T^2 + m_0^2} \cosh y - \mu}{T} \right]^{\frac{1}{q-1}} + S \right\}^{-q} dp_T, \quad (22)$$

where  $q$  is the entropy index which describes the degree of non-equilibrium of the collision system.

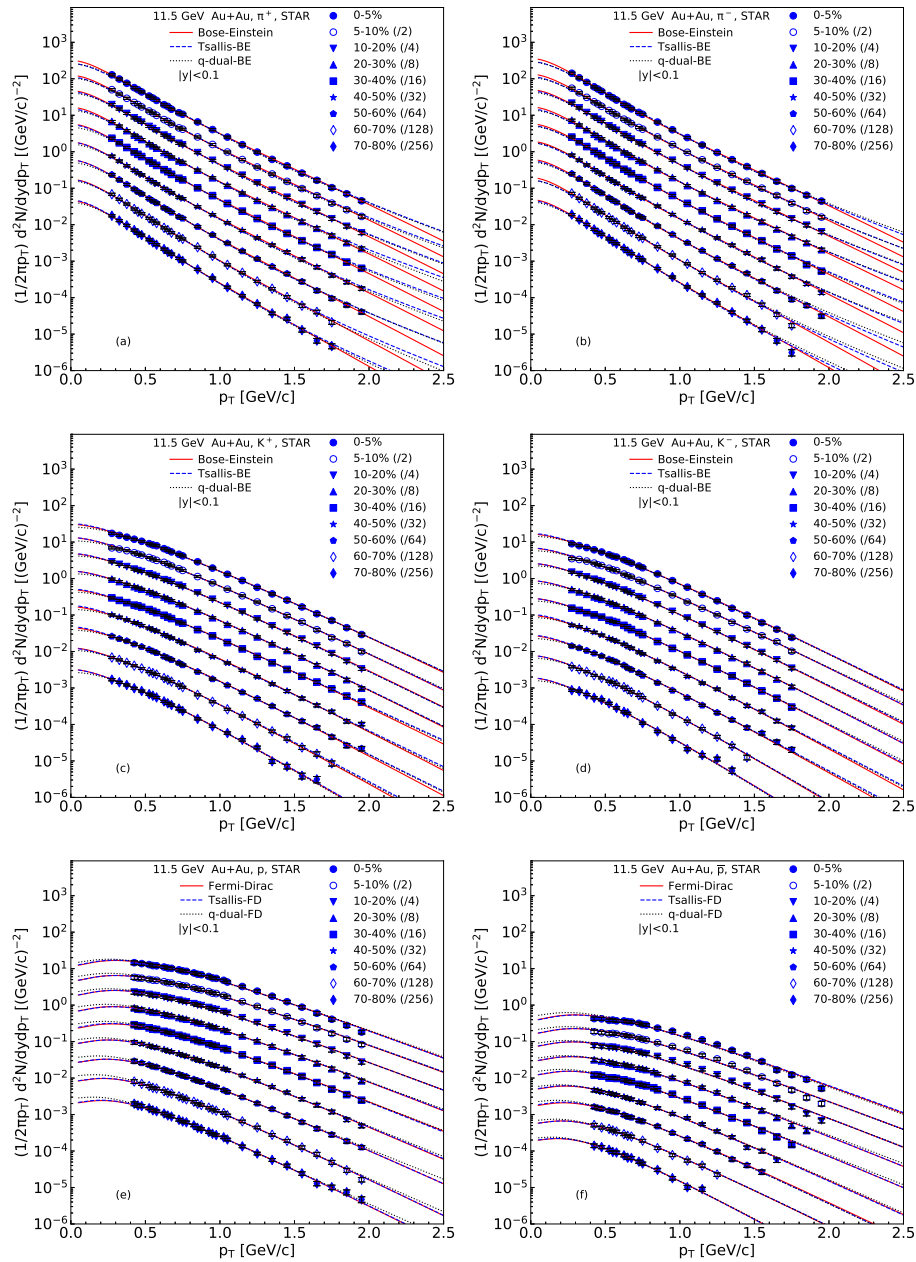


Figure 2. The invariant yields of (a)  $\pi^+$ , (b)  $\pi^-$ , (c)  $K^+$ , (d)  $K^-$ , (e)  $p$ , and (f)  $\bar{p}$  produced in  $|y| < 0.1$  in Au+Au collisions at  $\sqrt{s_{NN}} = 11.5$  GeV. Different symbols represent the experimental data measured by the STAR Collaboration [20] at RHIC with nine centrality percentage classes as those for Figure 1 and scaled by different quantities shown in the panels. The solid, dashed, and dotted curves are our results fitted by the distributions from the standard, Tsallis, and q-dual statistics, respectively.

Similar to the multi-component distributions in the standard statistics, one may structure the multi-component distributions in the Tsallis statistics which can be empirically covered by the distributions in the q-dual statistics which has the following related equations [37]

$$N = gV \int \frac{d^3p}{(2\pi)^3} \sum_{k=0}^{\infty} (-S)^k \left[ 1 + (k+1)(q-1) \frac{E - \mu}{T} \right]^{-\frac{q}{q-1}}, \quad (23)$$



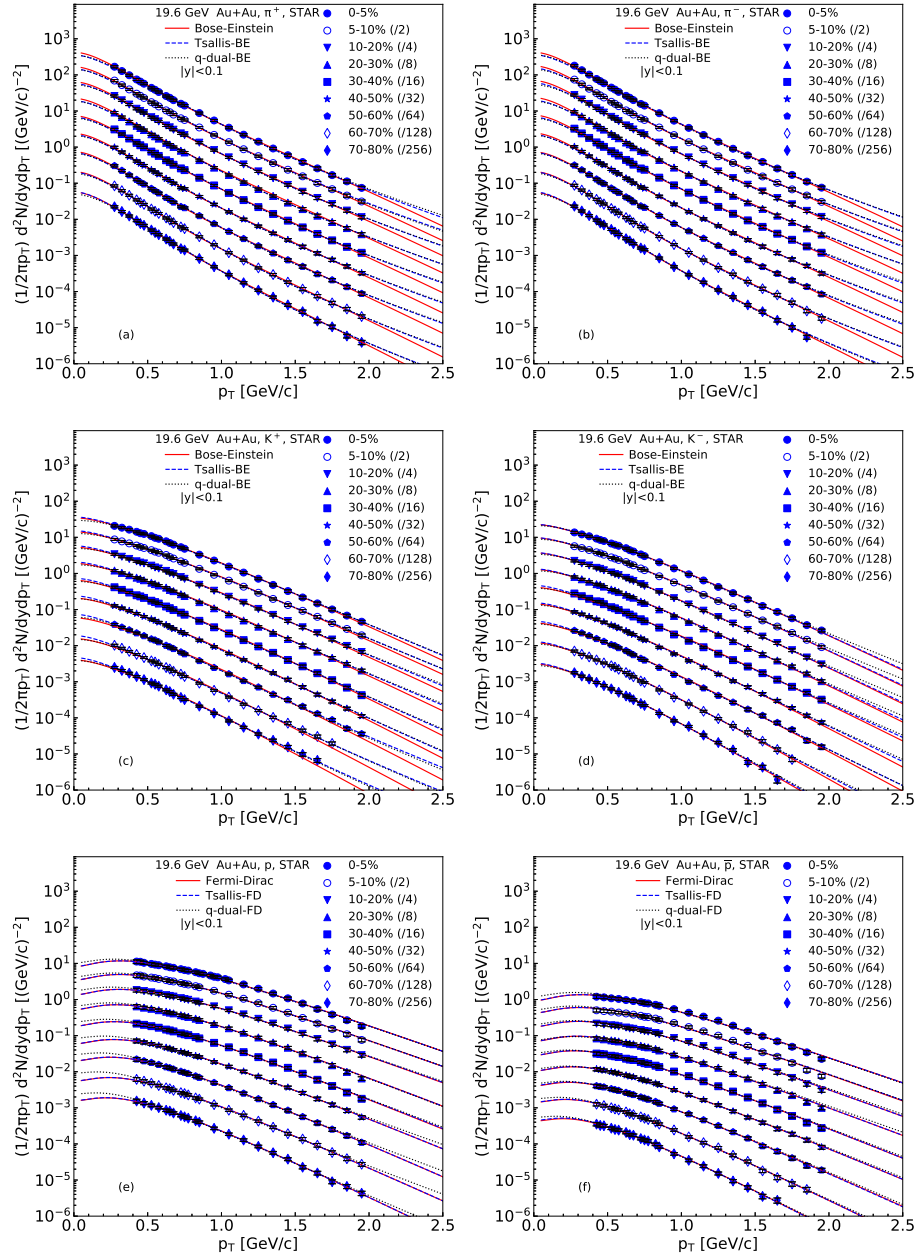


Figure 3. The invariant yields of (a)  $\pi^+$ , (b)  $\pi^-$ , (c)  $K^+$ , (d)  $K^-$ , (e)  $p$ , and (f)  $\bar{p}$  produced in  $|y| < 0.1$  in Au+Au collisions at  $\sqrt{s_{NN}} = 19.6$  GeV. Different symbols represent the experimental data measured by the STAR Collaboration [20] with nine centrality percentage classes as those for Figure 1 and scaled by different quantities shown in the panels. The solid, dashed, and dotted curves are our results fitted by the distributions from the standard, Tsallis, and q-dual statistics, respectively.

$$E \frac{d^3 N}{d^3 p} = \frac{gV}{(2\pi)^3} E \sum_{k=0}^{\infty} (-S)^k \left[ 1 + (k+1)(q-1) \frac{E-\mu}{T} \right]^{-\frac{q}{q-1}}, \quad (24)$$

$$\frac{dN}{dp} = \frac{2gV}{(2\pi)^2} p^2 \sum_{k=0}^{\infty} (-S)^k \left[ 1 + (k+1)(q-1) \frac{\sqrt{p^2 + m_0^2} - \mu}{T} \right]^{-\frac{q}{q-1}}, \quad (25)$$

$$\frac{d^2 N}{dy dp_T} = \frac{gV}{(2\pi)^2} p_T \sqrt{p_T^2 + m_0^2} \cosh y \sum_{k=0}^{\infty} (-S)^k \left[ 1 + (k+1)(q-1) \frac{\sqrt{p_T^2 + m_0^2} \cosh y - \mu}{T} \right]^{-\frac{q}{q-1}}, \quad (26)$$

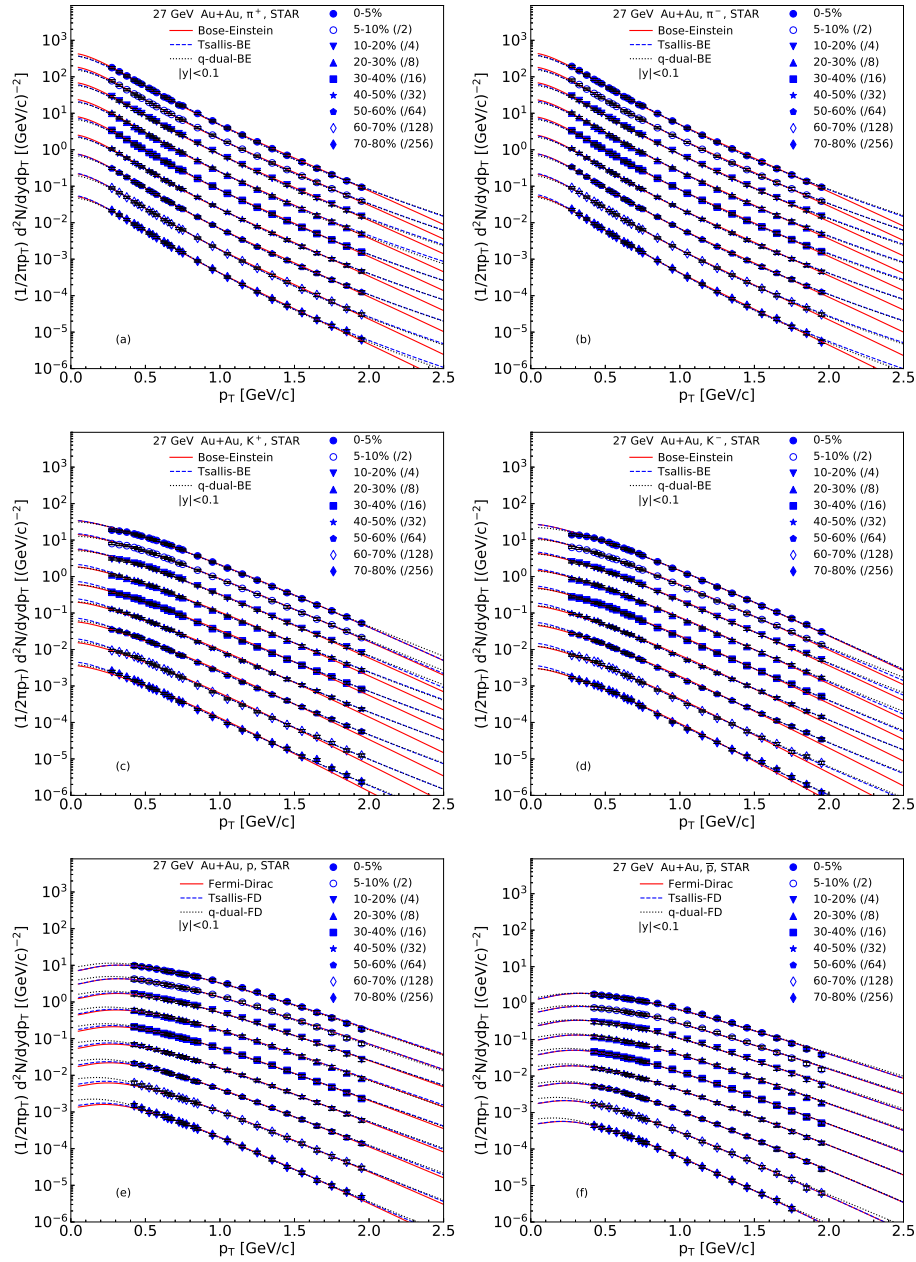


Figure 4. The invariant yields of (a)  $\pi^+$ , (b)  $\pi^-$ , (c)  $K^+$ , (d)  $K^-$ , (e)  $p$ , and (f)  $\bar{p}$  produced in  $|y| < 0.1$  in Au+Au collisions at  $\sqrt{s_{NN}} = 27$  GeV. Different symbols represent the experimental data measured by the STAR Collaboration [20] with nine centrality percentage classes as those for Figure 1 and scaled by different quantities shown in the panels. The solid, dashed, and dotted curves are our results fitted by the distributions from the standard, Tsallis, and q-dual statistics, respectively.

$$\frac{dN}{dp_T} = \frac{gV}{(2\pi)^2} p_T \sqrt{p_T^2 + m_0^2} \int_{y_{\min}}^{y_{\max}} \cosh y \sum_{k=0}^{\infty} (-S)^k \left[ 1 + (k+1)(q-1) \frac{\sqrt{p_T^2 + m_0^2} \cosh y - \mu}{T} \right]^{-\frac{q}{q-1}} dy, \quad (27)$$

$$\frac{dN}{dy} = \frac{gV}{(2\pi)^2} \int_0^{p_{T\max}} p_T \sqrt{p_T^2 + m_0^2} \cosh y \sum_{k=0}^{\infty} (-S)^k \left[ 1 + (k+1)(q-1) \frac{\sqrt{p_T^2 + m_0^2} \cosh y - \mu}{T} \right]^{-\frac{q}{q-1}} dp_T, \quad (28)$$

where  $k$  is an integer. Although the maximum  $k$  is  $\infty$ , it is enough if the maximum  $k$  is taken to be 10 in the calculation, where the contribution with  $k > 10$  is a small quantity which can be neglected.



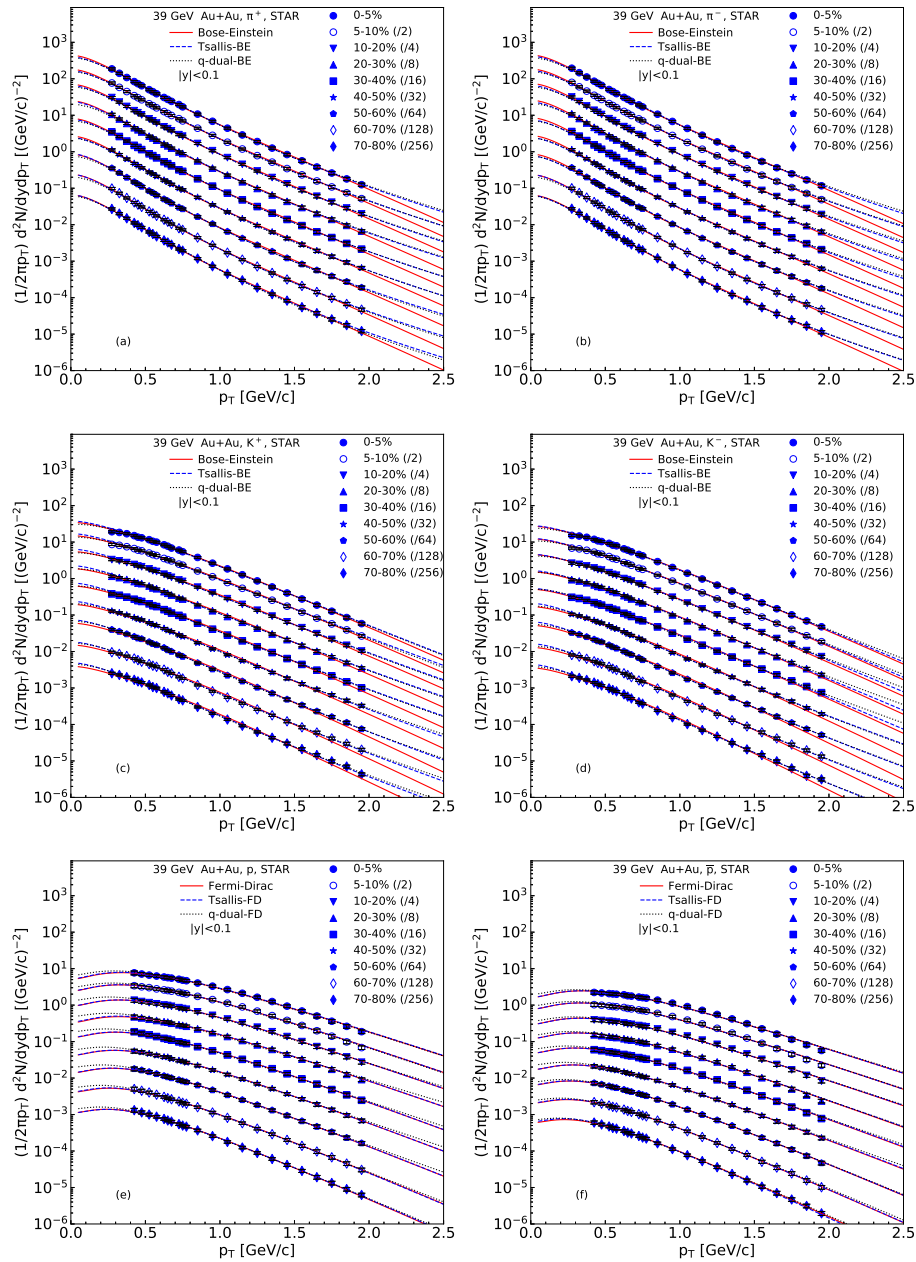


Figure 5. The invariant yields of (a)  $\pi^+$ , (b)  $\pi^-$ , (c)  $K^+$ , (d)  $K^-$ , (e)  $p$ , and (f)  $\bar{p}$  produced in  $|y| < 0.1$  in Au+Au collisions at  $\sqrt{s_{NN}} = 39$  GeV. Different symbols represent the experimental data measured by the STAR Collaboration [20] with nine centrality percentage classes as those for Figure 1 and scaled by different quantities shown in the panels. The solid, dashed, and dotted curves are our results fitted by the distributions from the standard, Tsallis, and q-dual statistics, respectively.

The experimental data analyzed herein are presented in terms of invariant yield allowing direct comparison with modelling results. Given that this work aims at comparing effective temperatures derived from standard statistical mechanics alongside Tsallis and q-dual statistics, our primary focus lies on extracting temperature values from these three frameworks. To differentiate between various temperatures associated with each statistical approach effectively we will denote them as  $T_{\text{Standard}}$ ,  $T_{\text{Tsallis}}$ , and  $T_{\text{q-dual}}$ , orderly. Furthermore if necessary entropy indices pertaining to Tsallis and q-dual statistics will be referred to as  $q_{\text{Tsallis}}$  and  $q_{\text{q-dual}}$  respectively.

In the extraction of effective temperatures, the chemical potential  $\mu$  is not a sensitive quantity due to its relatively small value compared to particle energy at the relevant RHIC energies. Nevertheless, there are at least two meth-

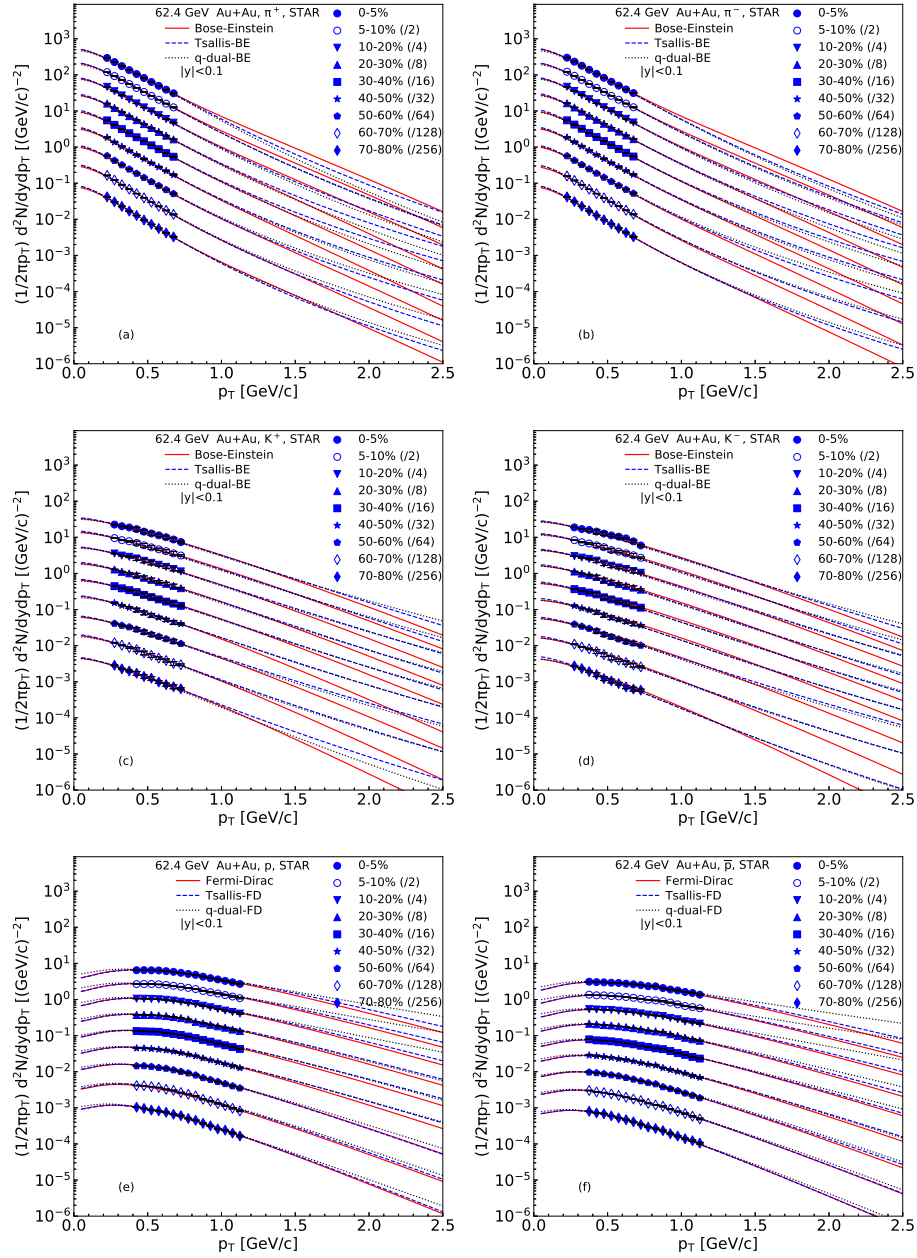


Figure 6. The invariant yields of (a)  $\pi^+$ , (b)  $\pi^-$ , (c)  $K^+$ , (d)  $K^-$ , (e)  $p$ , and (f)  $\bar{p}$  produced in  $|y| < 0.1$  in Au+Au collisions at  $\sqrt{s_{NN}} = 62.4$  GeV. Different symbols represent the experimental data measured by the STAR Collaboration [21] with nine centrality percentage classes as those for Figure 1 and scaled by different quantities shown in the panels. The solid, dashed, and dotted curves are our results fitted by the distributions from the standard, Tsallis, and q-dual statistics, respectively.

ods available for obtaining  $\mu$ . Let  $\mu_B$ ,  $\mu_S$ , and  $\mu_I$  denote the chemical potentials associated with baryon number, strangeness, and electric charge, respectively. The chemical potential  $\mu$  of a given particle can be expressed in terms of these three chemical potentials [38–43]. Alternatively, a more convenient method involves using the yield ratio of negatively charged to positively charged hadrons to determine  $\mu$  [22, 44–47]. We prefer to employ this second method as it is easier for our purposes.

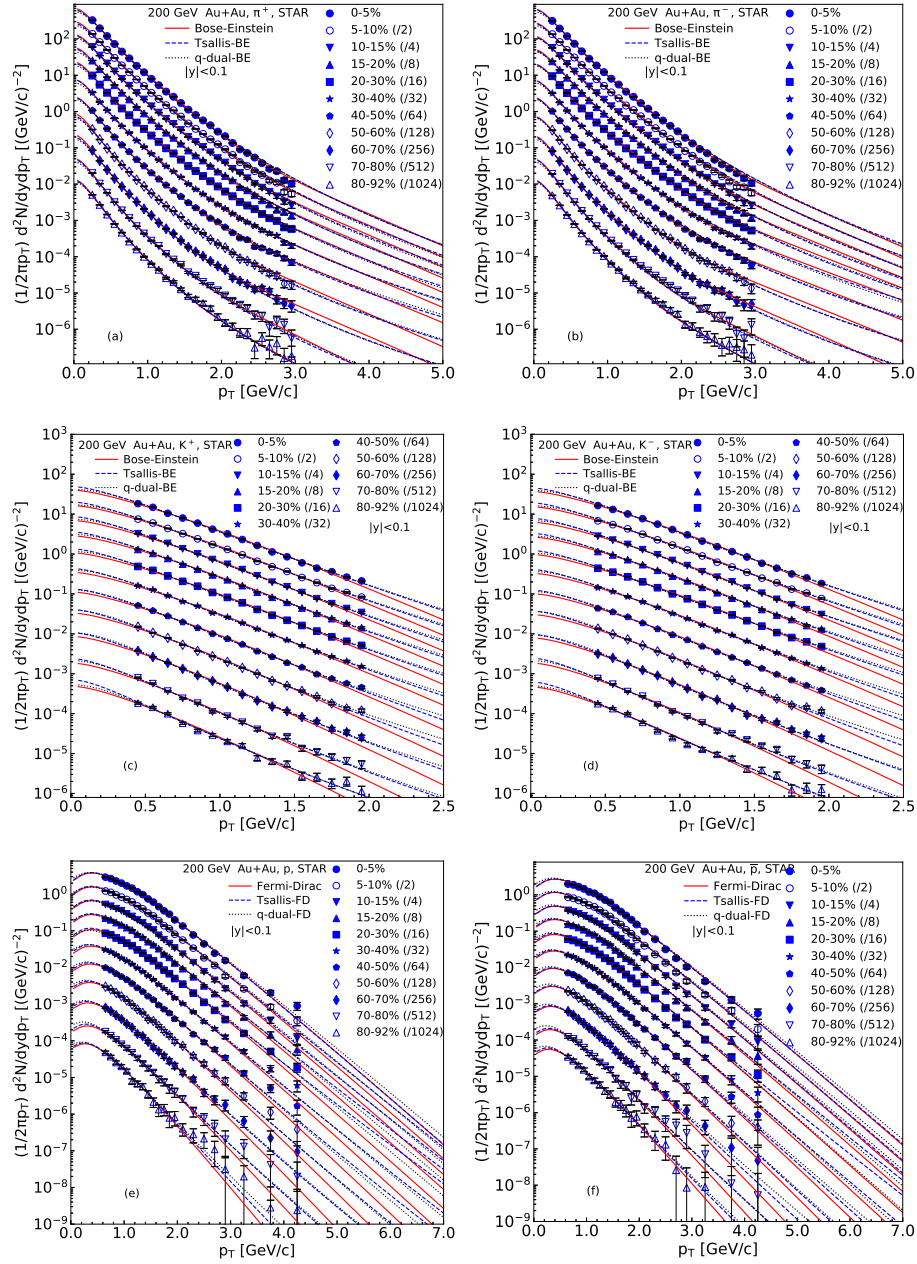


Figure 7. The invariant yields of (a)  $\pi^+$ , (b)  $\pi^-$ , (c)  $K^+$ , (d)  $K^-$ , (e)  $p$ , and (f)  $\bar{p}$  produced in  $|y| < 0.1$  in Au+Au collisions at  $\sqrt{s_{NN}} = 200$  GeV. Different symbols represent the experimental data measured by the STAR Collaboration [22] with eleven centrality percentage classes (0–5%, 5–10%, 10–15%, 15–20%, 20–30%, 30–40%, 40–50%, 50–60%, 60–70%, 70–80%, and 80–92%) and scaled by different quantities shown in the panels. The solid, dashed, and dotted curves are our results fitted by the distributions from the standard, Tsallis, and q-dual statistics, respectively.

### III. RESULTS AND DISCUSSION

#### A. Comparison with experimental data

Figures 1–7 present the invariant yields,  $(1/2\pi p_T)d^2N/dydp_T$ , for (a)  $\pi^+$ , (b)  $\pi^-$ , (c)  $K^+$ , (d)  $K^-$ , (e)  $p$ , and (f)  $\bar{p}$ , produced within  $|y| < 0.1$  in Au+Au collisions at  $\sqrt{s_{NN}} = 7.7, 11.5, 19.6, 27, 39, 62.4,$  and 200 GeV, respectively. Different symbols represent experimental data measured by the STAR Collaboration [20–22] at RHIC. In Figures 1–6

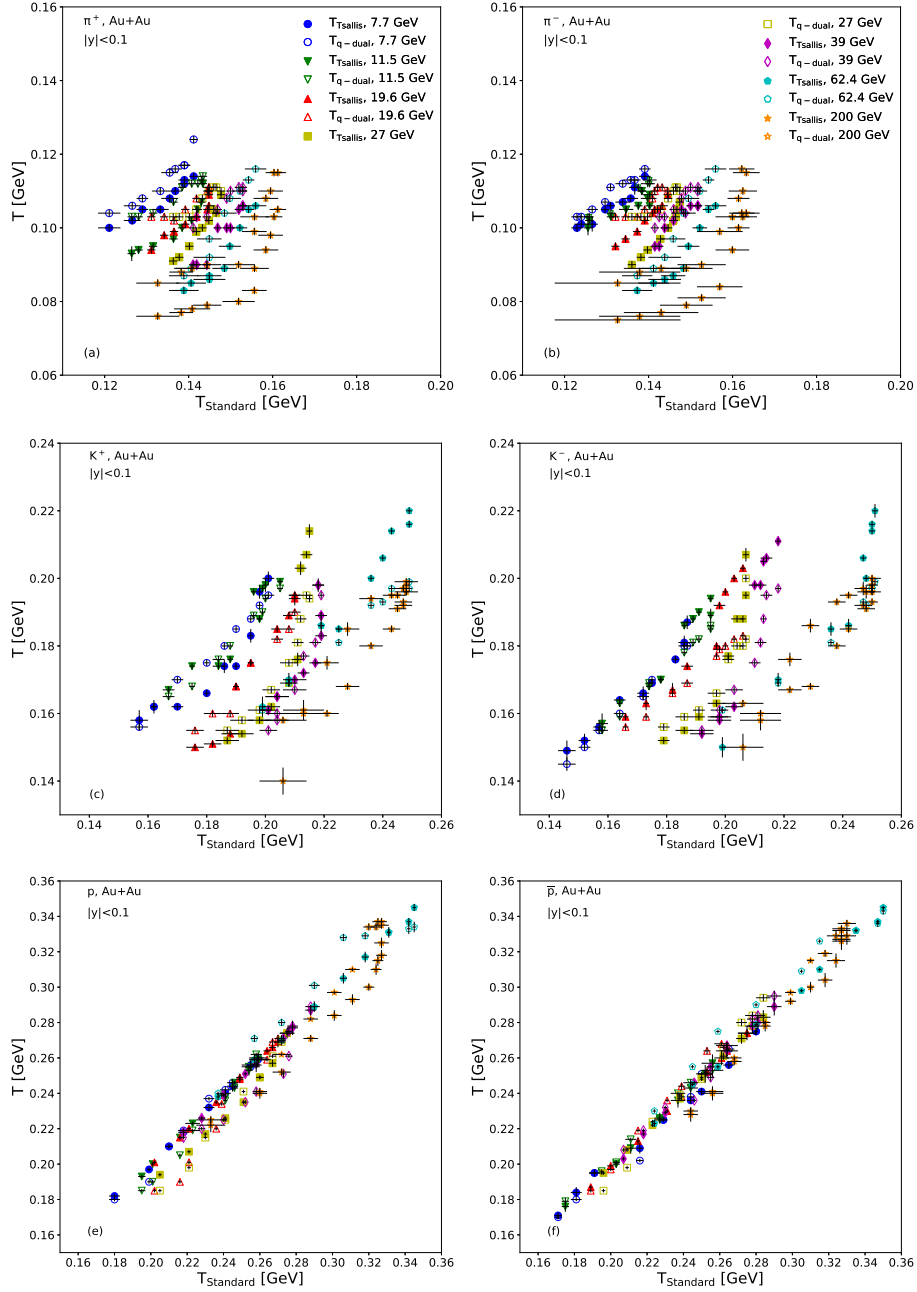


Figure 8. The dependence of  $T_{T_{\text{sallis}}}$  (closed symbols) and  $T_{q\text{-dual}}$  (open symbols) on  $T_{\text{Standard}}$  obtained from the spectra of (a)  $\pi^+$ , (b)  $\pi^-$ , (c)  $K^+$ , (d)  $K^-$ , (e)  $p$ , and (f)  $\bar{p}$  produced in Au+Au collisions with different centralities at RHIC. The symbols represent the results classified by different collision energies shown in the panels.

we utilize nine centrality percentage classes: 0–5%, 5–10%, 10–20%, 20–30%, 30–40%, 40–50%, 50–60%, 60–70%, and 70–80%. Figure 7 employs eleven centrality percentage classes: 0–5%, 5–10%, 10–15%, 15–20%, 20–30%, 30–40%, 40–50%, 50–60%, 60–70%, 70–80%, and 80–92%. For each centrality class presented in these figures, the data have been scaled by specific factors indicated in their respective panels for clarity.

In Figures 1–7, the solid, dashed, and dotted curves represent our results fitted using distributions from standard statistics, Tsallis statistics, and q-dual statistics, respectively. In standard statistics, either a two-component or three-component distribution is employed if a single-component distribution does not adequately fit the  $p_T$  spectra. Conversely, in both Tsallis and q-dual statistics, a single-component distribution suffices. In the fit, the least square

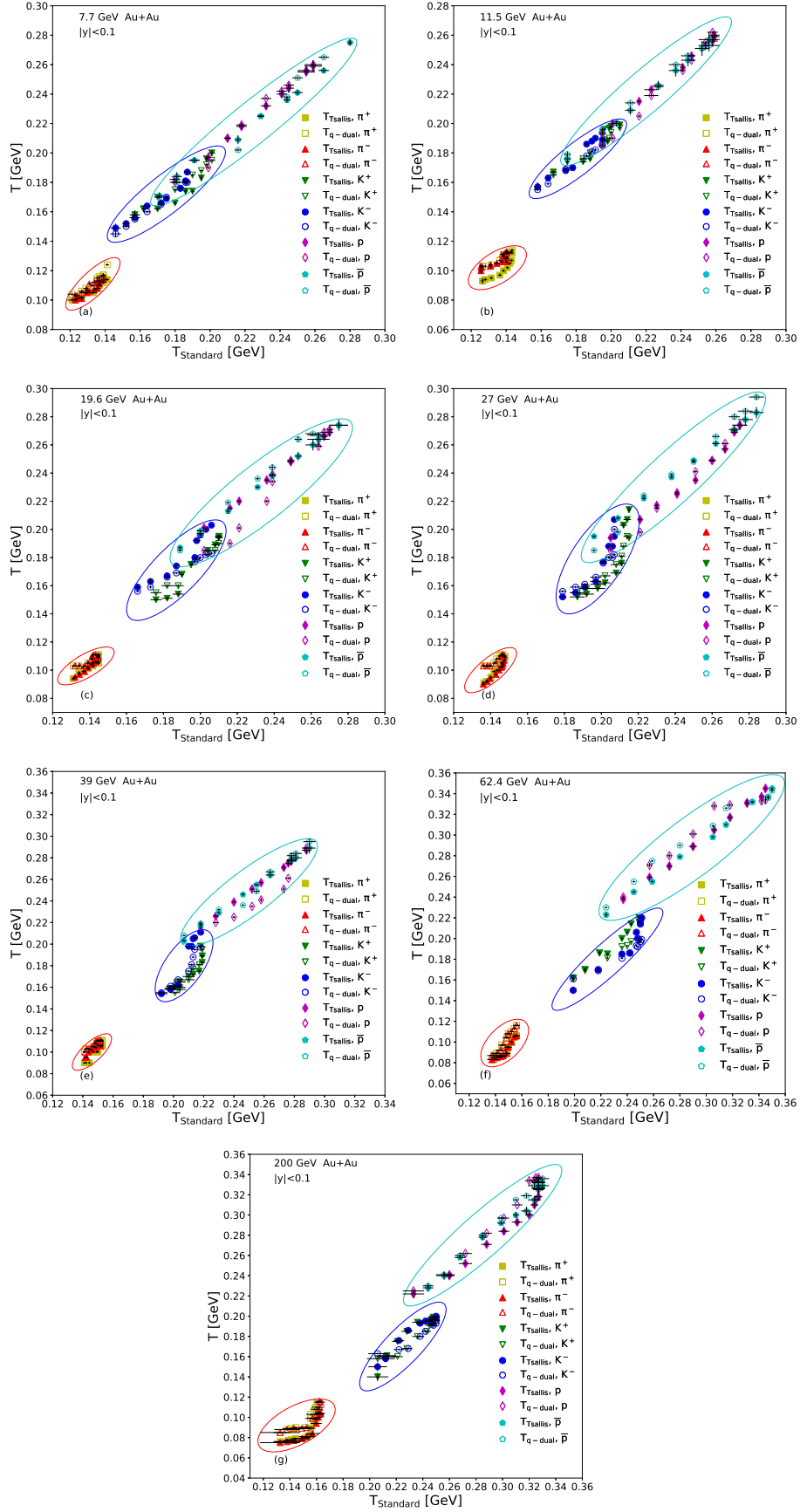


Figure 9. The dependence of  $T_{\text{Tsallis}}$  (closed symbols) and  $T_{\text{q-dual}}$  (open symbols) on  $T_{\text{Standard}}$  redisplayed in terms of  $\sqrt{s_{NN}}$  which equals to (a) 7.7, (b) 11.5, (c) 19.6, (d) 27, (e) 39, (f) 62.4, and (g) 200 GeV. The symbols represent the results classified by different hadrons shown in the panels.

method is performed to optimize the parameter values. In the three statistics, the main parameters are  $T_{\text{Standard}}$ ,  $T_{\text{Tsallis}}$ ,  $q_{\text{Tsallis}}$ ,  $T_{\text{q-dual}}$ , and  $q_{\text{q-dual}}$ . Here,  $T_{\text{Standard}} = k_1 T_1 + (1 - k_1) T_2$  or  $T_{\text{Standard}} = k_1 T_1 + k_2 T_2 + (1 - k_1 - k_2) T_3$ , in the case of considering two- or three-component distribution in the standard statistics.

In the distributions derived from both Tsallis and q-dual statistics, the free parameters include the effective temperature and entropy index. In contrast, for single-component distributions based on standard statistics, only the effective temperature serves as a free parameter. However, when considering two-component distributions, an additional two free parameters (temperature and fraction) are introduced; similarly, three-component distributions result in four extra free parameters (two temperatures and two fractions). As illustrated in Figures 1–7, experimental data from Au+Au collisions at varying centralities and energies, measured by the STAR Collaboration at RHIC, can be effectively fitted using distributions from standard statistics as well as Tsallis and q-dual statistics. Notably, in certain cases involving standard statistics, a two- or three-component distribution is necessary.

Numerous studies have examined how collision energy, particle mass, and event centrality influence effective temperature, kinetic freeze-out temperature, and entropy index; these findings have been documented in our previous work [48–50] as well as other literature [51–53]. It is worth noting that applications of q-dual statistics remain relatively scarce. The aforementioned studies indicate that effective temperatures and kinetic freeze-out temperatures exhibit slight increases or decreases, or may even saturate, as collision energy rises beyond 7.7 GeV. Additionally, these temperatures tend to increase with greater particle mass and event centrality levels; conversely, the entropy index shows an upward trend with increasing collision energy while decreasing with higher particle mass and event centrality.

This study does not present results pertaining to any specific exceptions previously discussed elsewhere; instead it focuses on comparing effective temperatures obtained through three types of statistical frameworks, specifically highlighting our limited use of q-dual statistics. While we have previously compared effective temperatures derived from Maxwell-Boltzmann statistics with those from Tsallis statistics [54, 55], this work aims to explore relationships among more extensive sets of effective temperatures and select a baseline from these comparisons. Naturally, the standard statistics can be regarded as the baseline due to its solid foundation and wide applicability.

## B. Tendencies of parameters

The dependence of  $T_{\text{Tsallis}}$  (closed symbols) and  $T_{\text{q-dual}}$  (open symbols) on  $T_{\text{Standard}}$ , derived from the spectra of (a)  $\pi^+$ , (b)  $\pi^-$ , (c)  $K^+$ , (d)  $K^-$ , (e)  $p$ , and (f)  $\bar{p}$  produced in Au+Au collisions with varying centralities at RHIC, is illustrated in Figure 8. In this figure, the symbols represent results categorized by different collision energies as shown in the panels. An alternative representation of these temperatures is provided in Figure 9, where the dependence of both  $T_{\text{Tsallis}}$  and  $T_{\text{q-dual}}$  on  $T_{\text{Standard}}$  is displayed as a function of  $\sqrt{s_{NN}}$  that equals to (a) 7.7, (b) 11.5, (c) 19.6, (d) 27, (e) 39, (f) 62.4, and (g) 200 GeV. Here again, the symbols denote results classified according to various hadrons depicted in the panels. The oblique elliptic curves serve to guide the eyes and differentiate between results for distinct particles.

From Figures 8 and 9, it can be observed that during the production of  $\pi^\pm$  in Au+Au collisions at energies of  $\sqrt{s_{NN}} = 62.4$  and 200 GeV, there is a notable increase in  $T_{\text{Standard}}$ , from peripheral collisions characterized by centrality ranges of 70–80% or 80–92% to semi-central collisions possessed centrality of 40–50%; however it subsequently changes slowly when transitioning further to central collisions carried centrality of 0–5%. Such behavior may imply potential formation conditions for quark-gluon plasma (QGP), analogous to processes like ice melting or water boiling.

In contrast to this trend for  $T_{\text{Standard}}$ , both  $T_{\text{Tsallis}}$  and  $T_{\text{q-dual}}$  exhibit significant increases at these specific energies and centralities examined here. Furthermore, a positive correlation appears evident between  $T_{\text{Tsallis}}$  and  $T_{\text{Standard}}$ , as well as between  $T_{\text{q-dual}}$  and  $T_{\text{Standard}}$ . This relationship holds true across other causes at different collision energies. The linear approximation may be disrupted due to entropy index influences inherent within both frameworks of Tsallis and q-dual statistics, regardless of whether QGP is formed or not.

In the production of  $\pi^\pm$  in Au+Au collisions with varying centralities at  $\sqrt{s_{NN}} = 7.7$ –39 GeV, as well as in the



production of  $K^\pm$  at  $\sqrt{s_{NN}} = 7.7\text{--}200$  GeV, approximate linear relationships between  $T_{\text{Tsallis}}$  and  $T_{\text{Standard}}$ , along with  $T_{\text{q-dual}}$  and  $T_{\text{Standard}}$ , exhibit dispersion across different collision energies. Conversely, for the production of  $p(\bar{p})$  in Au+Au collisions with differing centralities at  $\sqrt{s_{NN}} = 7.7\text{--}200$  GeV, these relationships appear more compact or nearly coincident across various collision energies. This discrepancy underscores the complexity inherent to high-energy collisions; however, it is noteworthy that the average temperature weighted by different particles closely aligns with that derived from the spectra of  $\pi^\pm$  due to their significantly high yield within this energy range.

Given that both  $T_{\text{Tsallis}}$  and  $T_{\text{q-dual}}$  demonstrate a significant growth when increasing centrality at 62.4 and 200 GeV, they are inadequate for accurately describing QGP formation in central and semi-central collisions at elevated energies. In contrast,  $T_{\text{Standard}}$  exhibits a rapid increase from peripheral to semi-central collisions before becoming slowly increase from semi-central to central collisions. This behavior of changing the slope relative to centrality is more suitable for characterizing QGP formation; nonetheless, it necessitates consideration of two- or three-component distributions. We contend that standard statistics, being fundamental, should receive greater emphasis in future research endeavors involving multi-component distributions.

### C. Further discussions

It is important to note that the experimental data utilized in this analysis encompass only a limited range of  $p_T$ , which seems to restrict the accurate determination of certain parameters. However, it is understood that high- $p_T$  particles are predominantly produced through hard scattering process, rather than soft excitation process. Generally, hard process should not contribute to the thermal parameters. If the experimental data were to cover a broader range of  $p_T$ , one might consider excluding high- $p_T$  particles in order to obtain thermal parameters as accurately as possible.

Furthermore, when compared with low- $p_T$  particle yield, the yield of high- $p_T$  particles is much smaller and can often be disregarded. Even if the contribution of high- $p_T$  are not excluded in extracting thermal parameters, their effects can be neglected. Indeed, the hard scattering is associated with the heavy tail observed in the data. While this observation holds true for distributions derived from standard statistics, it is important to note that distributions based on Tsallis and q-dual statistics can effectively describe the nearly entire range of  $p_T$  distribution. Nevertheless, as we have indicated, both including and excluding high  $p_T$  spectra have minimal impact on the extraction of thermal parameters.

Usually, the peak of the  $p_T$  distribution occurs in very low region, in which the yield is primarily influenced by strong decays from high-mass resonances and weak decays from heavy flavor hadrons [56], both of which should be excluded from thermal distributions. Conversely, effective temperature is mainly determined by the inverse slope of the distribution arising from soft excitation process. The absence of data covering this peak does not significantly impact our ability to determine temperature accurately across all methodologies employed in this study. In fact, similar approaches have been documented in previous literature such as refs. [20–22].

As discussed in the preceding section, the entropy index plays a crucial role in extracting effective temperature within Tsallis and q-dual statistics frameworks. Several studies have highlighted correlations among adjustable parameters [57–59], particularly within Tsallis statistics and similar non-extensive statistical models; these studies indicate a negative correlation between effective temperature and entropy index. These correlations influence the temperature values obtained, which are a key parameter in this study. To mitigate the impact of correlations among different parameters, one not only applies the least squares method but also allows for varying selected  $p_T$  ranges for different particles when extracting thermal parameters [20–22]. What we do in this study is the application of the least squares method.

While a standard distribution can effectively describe a single source at a given excitation degree or temperature, a multi-component standard distribution characterizes the system with multiple sources or temperatures that reflect temperature fluctuation occurring among these sources [60]. Due to differing temperatures, interactions between various sources may occur through heat energy exchange. Consequently, the collision system evolves toward an equilibrium state; however, it ultimately remains in an approximate equilibrium state. The exchange of heat energy

among distinct sources leads to coupling of their entropy functions. Thus, the total entropy is represented as the sum of entropies from various sources along with their couplings.

The multi-component standard distribution can be described using non-extensive distributions derived from Tsallis statistics. In explaining the origin of this non-extensive distribution, temperature fluctuation within the multi-component standard distribution is a candidate [60], which corresponds to specific temperature in Tsallis statistics. The degree of non-equilibrium among different sources is characterized by an entropy index within this framework. Given that multiple sources are produced in high-energy collisions, it follows that non-extensive Tsallis statistics may represent one of the fundamental features inherent in such process [57]. Furthermore, there exists a relationship between non-extensive Tsallis distributions and Boltzmann's factor through continuous summation weighted by factors defined by Euler–Gamma function [60].

Before presenting our summary and conclusions, we would like to emphasize that the introduction of multi-source mechanisms within the multi-source thermal model [23–25] does not significantly alter the relationships among  $T_{\text{Tsallis}}$ ,  $T_{\text{q-dual}}$ , and  $T_{\text{Standard}}$ . In our view, these temperature relationships are inherent due to the specific forms used in modelling  $p_T$  distributions. The incorporation of multi-source mechanisms may yield a multi-component distribution capable of fitting experimental  $p_T$  spectra with high accuracy. Furthermore, introducing these mechanisms can provide a clearer physical picture that reflects the complexities involved in high-energy collisions.

#### IV. SUMMARY AND CONCLUSIONS

The invariant yields of  $\pi^\pm$ ,  $K^\pm$ , and  $p(\bar{p})$  produced in  $|y| < 0.1$  in Au+Au collisions with various centralities at  $\sqrt{s_{NN}} = 7.7, 11.5, 19.6, 27, 39, 62.4,$  and 200 GeV measured by the STAR Collaboration at RHIC have been analyzed using distributions derived from standard statistics as well as Tsallis and q-dual statistics. In certain cases, a two- or three-component distribution within standard statistics is necessary for accurate representation. The experimental data can be effectively fitted using these related distributions. Effective temperature parameters such as  $T_{\text{Standard}}$ ,  $T_{\text{Tsallis}}$ , and  $T_{\text{q-dual}}$  are extracted through fitting the spectra of identified light charged hadrons.

In the production of  $\pi^\pm$  in collisions at  $\sqrt{s_{NN}} = 62.4$  and 200 GeV, it is observed that while  $T_{\text{Standard}}$  increases rapidly initially before changing more gradually, both  $T_{\text{Tsallis}}$  and  $T_{\text{q-dual}}$  exhibit significant increases with rising centrality levels. The anticipated approximate linear relationships between  $T_{\text{Tsallis}}$  and  $T_{\text{Standard}}$ , as well as between  $T_{\text{q-dual}}$  and  $T_{\text{Standard}}$ , are disrupted due to the influence of entropy index associated with QGP formation; however, similar approximate linear relationships do exist in other scenarios.

For the production of  $\pi^\pm$  across different centralities at  $\sqrt{s_{NN}} = 7.7\text{--}39$  GeV, along with that of  $K^\pm$  over a range from  $\sqrt{s_{NN}} = 7.7$  to 200 GeV, there appears to be a dispersion in the approximate linear relationships between both  $T_{\text{Tsallis}}$  versus  $T_{\text{Standard}}$ , as well as  $T_{\text{q-dual}}$  versus  $T_{\text{Standard}}$  across varying collision energies. Conversely, for  $p(\bar{p})$  production under different centralities spanning from  $\sqrt{s_{NN}} = 7.7$  to 200 GeV, these aforementioned approximate linear relationships remain compacted or nearly coincide across distinct collision energies.

If QGP is formed in central and semi-central Au+Au collisions at  $\sqrt{s_{NN}} = 62.4$  and 200 GeV, one would expect the temperature to display a slowly changing trend as a function of centrality. However, both  $T_{\text{Tsallis}}$  and  $T_{\text{q-dual}}$  exhibit a significant increase, and  $T_{\text{Standard}}$  demonstrates a slowly increase, with increasing centrality. We argue that standard statistics, characterized by multi-component distributions, are more appropriate for describing QGP formation and should receive greater emphasis in future research.

#### Acknowledgements

The work of Shanxi Group was supported by the National Natural Science Foundation of China under Grant No. 12147215, the Shanxi Provincial Basic Research Program (Natural Science Foundation) under Grant No. 202103021224036, and the Fund for Shanxi “1331 Project” Key Subjects Construction. The work of P.P.Y. was supported by the Shanxi Provincial Basic Research Program (Natural Science Foundation) under Grant No. 202203021222308, the Doctoral Scientific Research Foundations of Shanxi Province and Xinzhou Normal University,

and the Academic Leading Specialist Project of Xinzhou Normal University under Grant Nos. 2024RC10 and 2024RC10B. The work of K.K.O. was supported by the Agency of Innovative Development under the Ministry of Higher Education, Science and Innovations of the Republic of Uzbekistan within the fundamental project No. F3-20200929146 on analysis of open data on heavy-ion collisions at RHIC and LHC.

**Data Availability Statement** This manuscript has associated data in a data repository. [Author’s comment: The data analyzed in this manuscript were obtained from <https://www.hepdata.net/>, a freely accessible repository.]

**Code Availability Statement** This manuscript has no associated code/software. [Author’s comment: Code/Software sharing not applicable to this article as no code/software was generated or analysed during the current study].

**Disclosure** The funding agencies have no role in the design of the study; in the collection, analysis, or interpretation of the data; in the writing of the manuscript; or in the decision to publish the results.

**Conflicts of Interest** The authors declare that there are no conflict of interest regarding the publication of this paper.

**Ethical Standards** This research complies with the ethical standards.

- 
- [1] T.S. Biró, Is there a temperature? conceptual challenges at high energy, acceleration and complexity, Spring, 2011
- [2] M. Waqas, G.X. Peng, M. Ajaz, A.H. Ismail, Z. Wazir, L.L. Li, Extraction of different temperatures and kinetic freeze-out volume in high energy collisions. *J. Phys. G* **49**, 095102 (2022)
- [3] M. Csanad, I. Majer, Equation of state and initial temperature of quark gluon plasma at RHIC. *Cent. Eur. J. Phys.* **10**, 850–857 (2012)
- [4] P. Braun-Munzinger, J. Stachel, C. Wetterich, Chemical freeze-out and the QCD phase transition temperature. *Phys. Lett. B* **596**, 61–69 (2004)
- [5] F.A. Flor, G. Olinger, R. Bellwied, System size and flavour dependence of chemical freeze-out temperatures in ALICE data from pp, pPb and PbPb collisions at LHC energies. *Phys. Lett. B* **834**, 137473 (2022)
- [6] M. Waqas, G.X. Peng, Z. Wazir, H.L. Lao, Analysis of kinetic freeze out temperature and transverse flow velocity in nucleus-nucleus and proton-proton collisions at same center of mass energy. *Int. J. Mod. Phys. E* **30**, 2150061 (2021)
- [7] Yu.B. Ivanova, V.N. Russkikh, Transverse-mass effective temperature in heavy-ion collisions from AGS to SPS. *Eur. Phys. J. A* **37**, 139–142 (2008)
- [8] F.G. Gardim, G. Giacalone, M. Luzum, J.Y. Ollitrault, Thermodynamics of hot strong-interaction matter from ultrarelativistic nuclear collisions. *Nat. Phys.* **16**, 615–619 (2020)
- [9] L.J. Gutay, A.S. Hirsch, C. Pajares, R.P. Scharenberg, B.K. Srivastava, De-confinement in small systems: Clustering of color sources in high multiplicity  $\bar{p}p$  collisions at  $\sqrt{s} = 1.8$  TeV. *Int. J. Mod. Phys. E* **24**, 1550101 (2015)
- [10] R.P. Scharenberg, B.K. Srivastava, C. Pajares, Exploring the initial stage of high multiplicity proton–proton collisions by determining the initial temperature of the quark-gluon plasma. *Phys. Rev. D* **100**, 114040 (2019)
- [11] P. Sahoo, S. De, S.K. Tiwari, R. Sahoo, Energy and centrality dependent study of deconfinement phase transition in a color string percolation approach at RHIC energies. *Eur. Phys. J. A* **54**, 136 (2018)
- [12] H. Zheng, L.L. Zhu, Comparing the Tsallis distribution with and without thermodynamical description in p+p collisions. *Adv. High Energy Phys.* **2016**, 9632126 (2016)
- [13] Z.B. Tang, Y.C. Xu, L.J. Ruan, G. van Buren, F.Q. Wang, Z.B. Xu, Spectra and radial flow in relativistic heavy ion collisions with Tsallis statistics in a blastwave description. *Phys. Rev. C* **79**, 051901(R) (2009)

- [14] C. Tsallis, Possible generalization of Boltzmann-Gibbs statistics. *J. Stat. Phys.* **52**, 479–487 (1988)
- [15] C. Tsallis, Nonadditive entropy and nonextensive statistical mechanics – an overview after 20 years. *Braz. J. Phys.* **39**, 337–356 (2009)
- [16] T.S. Biró, G. Purcsel, K. Urmösy, Non-extensive approach to quark matter. *Eur. Phys. J. A* **40**, 325–340 (2009)
- [17] J. Cleymans, M.W. Paradza, Statistical approaches to high energy physics: chemical and thermal freeze-outs. *Physics* **2**, 654–664 (2020)
- [18] A.S. Parvan, Equivalence of the phenomenological Tsallis distribution to the transverse momentum distribution of q-dual statistics. *Eur. Phys. J. A* **56**, 106 (2020)
- [19] J. Cleymans, D. Worku, Relativistic thermodynamics: transverse momentum distributions in high-energy physics. *Eur. Phys. J. A* **48**, 160 (2012)
- [20] L. Adamczyk, J.K. Adkins, G. Agakishiev, M.M. Aggarwal, Z. Ahammed, N.N. Ajitanand, I. Alekseev, D.M. Anderson, R. Aoyama, A. Aparin, et al., STAR Collaboration, Bulk properties of the medium produced in relativistic heavy-ion collisions from the beam energy scan program. *Phys. Rev. C* **96**, 044904 (2017)
- [21] B.I. Abelev, M.M. Aggarwal, Z. Ahammed, B.D. Anderson, D. Arkhipkin, G.S. Averichev, Y. Bai, J. Balewski, O. Baranikova, L.S. Barnby, et al., STAR Collaboration, Systematic measurements of identified particle spectra in pp, d+Au, and Au+Au collisions at the STAR detector. *Phys. Rev. C* **79**, 034909 (2009)
- [22] S.S. Adler, S. Afanasiev, C. Aidala, N.N. Ajitanand, Y. Akiba, J. Alexander, R. Amirkas, L. Aphecetche, S.H. Aronson, R. Auerbeck, et al., STAR Collaboration, Identified charged particle spectra and yields in Au+Au collisions at  $\sqrt{s_{NN}} = 200$  GeV. *Phys. Rev. C* **69**, 034909 (2004)
- [23] F.H. Liu, Unified description of multiplicity distributions of final-state particles produced in collisions at high energies. *Nucl. Phys. A* **810**, 159–172 (2008)
- [24] F.H. Liu, J.S. Li, Isotopic production cross section of fragments in  $^{56}\text{Fe}+p$  and  $^{136}\text{Xe}(^{124}\text{Xe})+\text{Pb}$  reactions over an energy range from 300A to 1500A MeV. *Phys. Rev. C* **78**, 044602 (2008)
- [25] F.H. Liu, Dependence of charged particle pseudorapidity distributions on centrality and energy in  $p(d)A$  collisions at high energies. *Phys. Rev. C* **78**, 014902 (2008)
- [26] M. Suleymanov, The meaning behind observed  $p_T$  regions at the LHC energies. *Int. J. Mod. Phys. E* **27**, 1850008 (2018)
- [27] M. Suleymanov, Some properties of the  $p_T$  regions observed at the LHC energies. *Int. J. Mod. Phys. E* **28**, 1950084 (2019)
- [28] M. Suleymanov, Energy and mass dependencies for the characteristics of  $p_T$  regions observed at LHC energies. *Phys. Part. Nucl.* **54**, 693–702 (2023)
- [29] A.N. Mishra, A. Ortiz, G. Paic, Intriguing similarities of high- $p_T$  particle production between  $pp$  and  $A-A$  collisions. *Phys. Rev. C* **99**, 034911 (2019)
- [30] E.K.G. Sarkisyan, A.S. Sakharov, Multihadron production features in different reactions. *AIP Conf. Proc.* **828**, 35–41 (2006)
- [31] A.N. Mishra, R. Sahoo, E.K.G. Sarkisyan, A.S. Sakharov, Effective-energy budget in multiparticle production in nuclear collisions. *Eur. Phys. J. C* **74**, 3147 (2014) and Erratum. *Eur. Phys. J. C* **75**, 70 (2015)
- [32] E.K.G. Sarkisyan, A.S. Sakharov, Relating multihadron production in hadronic and nuclear collisions. *Eur. Phys. J. C* **70**, 533–541 (2010)
- [33] E.K.G. Sarkisyan, A.N. Mishra, R. Sahoo, A.S. Sakharov, Multihadron production dynamics exploring the energy balance in hadronic and nuclear collisions. *Phys. Rev. D* **93** 054046 (2016) and Erratum. *Phys. Rev. D* **93**, 079904 (2016)
- [34] E.K.G. Sarkisyan, A.N. Mishra, R. Sahoo, A.S. Sakharov, Centrality dependence of midrapidity density from GeV to TeV heavy-ion collisions in the effective-energy universality picture of hadroproduction. *Phys. Rev. D* **94**, 011501(R) (2016)
- [35] E.K.G. Sarkisyan, A.N. Mishra, R. Sahoo, A.S. Sakharov, Effective-energy universality approach describing total multiplicity centrality dependence in heavy-ion collisions. *EPL (Europhys. Lett.)* **127**, 62001 (2019)
- [36] P. Castorina, A. Iorio, D. Lanteri, H. Satz, M. Spusta, Universality in hadronic and nuclear collisions at high energy. *Phys. Rev. C* **101**, 054902 (2020)
- [37] A.S. Parvan, Equivalence of the phenomenological Tsallis distribution to the transverse momentum distribution of q-dual statistics. *Eur. Phys. J. A* **56**, 106 (2020)
- [38] P. Braun-Munzinger, J. Stachel, J.P. Wessels, N. Xu, Thermal equilibration and expansion in nucleus-nucleus collisions at the AGS. *Phys. Lett. B* **344**, 43–48 (1995)

- [39] A. Andronic, P. Braun-Munzinger, J. Stachel, Thermal hadron production in relativistic nuclear collisions: The hadron mass spectrum, the horn, and the QCD phase transition. *Phys. Lett. B* **673**, 142–145 (2009)
- [40] J. Cleymans, H. Oeschler, K. Redlich, Influence of impact parameter on thermal description of relativistic heavy ion collisions at (1–2)A GeV. *Phys. Rev. C* **59**, 1663–1673 (1999)
- [41] P. Braun-Munzinger, I. Heppe, J. Stachel, Chemical equilibration in Pb+Pb collisions at the SPS. *Phys. Lett. B* **465**, 15–20 (1999)
- [42] J. Manninen, F. Becattini, Chemical freeze-out in ultra-relativistic heavy ion collisions at  $\sqrt{s_{NN}} = 130$  and 200 GeV. *Phys. Rev. C* **78**, 054901 (2008)
- [43] A. Andronic, P. Braun-Munzinger, K. Redlich, Decoding the phase structure of QCD via particle production at high energy. *Nature* **561**, 321–330 (2018)
- [44] P. Koch, J. Rafelski, W. Greiner, Strange hadron in hot nuclear matter. *Phys. Lett. B* **123**, 321–330 (1983)
- [45] P. Braun-Munzinger, D. Magestro, K. Redlich, J. Stachel, Hadron production in Au-Au collisions at RHIC. *Phys. Lett. B* **518**, 41–46 (2001)
- [46] F.H. Liu, T. Tian, H. Zhao, B.C. Li, Extracting chemical potentials of quarks from ratios of negatively/positively charged particles in high-energy collisions. *Eur. Phys. J. A* **50**, 62 (2014)
- [47] H.L. Lao, Y.Q. Gao, F.H. Liu, Light particle and quark chemical potentials from negatively to positively charged particle yield ratios corrected by removing strong and weak decays. *Adv. High Energy Phys.* **2020**, 5064737 (2020)
- [48] P.P. Yang, F.H. Liu, K.K. Olimov, Rapidity and energy dependencies of temperatures and volume extracted from identified charged hadron spectra in proton–proton collisions at a Super Proton Synchrotron (SPS). *Entropy* **25**, 1571 (2023)
- [49] P.P. Yang, M.Y. Duan, F.H. Liu, R. Sahoo, Analysis of identified particle transverse momentum spectra produced in pp, p–Pb and Pb–Pb collisions at the LHC using TP-like function. *Symmetry* **14**, 1530 (2022)
- [50] L.L. Li, F.H. Liu, K.K. Olimov, Excitation functions of Tsallis-like parameters in high-energy nucleus-nucleus collisions. *Entropy* **23**, 478 (2021)
- [51] M. Badshah, H.I. Alrebdi, M. Waqas, M. Ajaz, M.B. Ammar, Centrality-dependent analysis of hadrons and light nuclei for phase transition insights in intermediate-energy Au–Au collisions. *Eur. Phys. J. A* **60**, 139 (2024)
- [52] M. Badshah, M. Waqas, M. Ajaz, W. Bietenholz, H.I. Alrebdi, M.B. Ammar, Thermodynamic signatures and phase transitions in high-energy Au–Au collision. *J. Phys. G* **51**, 065109 (2024)
- [53] M. Badshah, M. Ajaz, M. Waqas, H. Younis, Evolution of effective temperature, kinetic freeze-out temperature and transverse flow velocity in pp collision. *Phys. Scr.* **98**, 115306 (2023)
- [54] F.H. Liu, Y.Q. Gao, B.C. Li, Comparing two-Boltzmann distribution and Tsallis statistics of particle transverse momentums in collisions at LHC energies. *Eur. Phys. J. A* **50**, 123 (2014)
- [55] Y.Q. Gao, F.H. Liu, Comparing Tsallis and Boltzmann temperatures from relativistic heavy ion collider and large hadron collider heavy-ion data. *Indian J. Phys.* **90**, 319–334 (2016)
- [56] N. Yu, X. Luo, Particle decay from statistical thermal model in high-energy nucleus-nucleus collisions. *Eur. Phys. J. A* **55**, 26 (2016)
- [57] J.O. Costa, I. Aguiar, J.L. Barauna, E. Megías, A. Deppman, T.N. da Silva, D.P. Menezes, Non-extensive statistics in Au-Au collisions. *Phys. Lett. B* **854**, 138727 (2024)
- [58] M. Waqas, W. Bietenholz, M. Bouzidi, M. Ajaz, A.H. Ismail, T. Saidani, Analyzing the correlation between thermal and kinematic parameters in various multiplicity classes within 7 and 13 TeV pp collisions. *J. Phys. G* **51**, 075102 (2024)
- [59] M. Waqas, G.X. Peng, M. Ajaz, A.H. Ismail, E.A. Dawi, Analyses of the collective properties of hadronic matter in Au-Au collisions at 54.4 GeV. *Phys. Rev. D* **106**, 075009 (2022)
- [60] J.Y. Chen, M.Y. Duan, F.H. Liu, K.K. Olimov, Multi-source thermal model describing multi-region structure of transverse momentum spectra of identified particles and parameter dynamics of system evolution in relativistic collisions. *Indian J. Phys.* **98**, 2493–2505 (2024)